International Journal of Nanomedicine

Dovepress
Taylor & Francis Group

Open Access Full Text Article

ORIGINAL RESEARCH

Glioma Cell Membrane–Coated $CaCO_3$ Nanoparticles for Localized Postoperative Chemo–Calcium Overload Therapy to Prevent Glioma Recurrence

Shiqiang Hou[1,*], Chao Zhang[1,*], Yu Wang[1,*], Xinwei Li[1], Zihao Wang[1], Jing Wang[1], Minfeng Yang[2], Zhen Liang[3], Ning Lin[1]

[1]Department of Neurosurgery, The Affiliated Chuzhou Hospital of Anhui Medical University, The First People's Hospital of Chuzhou, Chuzhou, 239001, People's Republic of China; [2]School of Public Health, Nantong University, Nantong, 226004, People's Republic of China; [3]School of Biomedical Engineering, Anhui Medical University, Hefei, 230032, People's Republic of China

*These authors contributed equally to this work

Correspondence: Ning Lin, Department of Neurosurgery, The Affiliated Chuzhou Hospital of Anhui Medical University, The First People's Hospital of Chuzhou, Chuzhou, 239001, People's Republic of China, Email linning@ahmu.edu.cn; Zhen Liang, School of Biomedical Engineering, Anhui Medical University, Hefei, 230032, People's Republic of China, Email zliang@ahmu.edu.cn

Background: Postoperative recurrence of glioma remains a major clinical challenge due to the blood-brain barrier and an immunosuppressive tumor microenvironment, necessitating innovative local treatment strategies.

Methods: We developed a biomimetic nanoplatform (CaDM) by coating doxorubicin (DOX)-loaded calcium carbonate nanoparticles with a glioma cell membrane. This construct was then integrated with the clinical hemostatic agent Surgiflo to create an in-situ forming depot for localized application into the tumor resection cavity.

Results: The CaDM nanoparticles exhibited excellent acid-responsive degradation, enabling simultaneous release of DOX and Ca^{2+} in the tumor microenvironment. This co-delivery initiated a potent synergistic antitumor effect: DOX induced direct cytotoxicity and immunogenic cell death (ICD), while Ca^{2+} influx triggered calcium overload, mitochondrial damage, and tumor vascular thrombosis. Furthermore, $CaCO_3$ degradation neutralized the acidic microenvironment, downregulating cathepsin B to reverse immunosuppression. In the postoperative glioma model, CaDM@Surgiflo significantly suppressed tumor recurrence and extended the median survival of mice from 14 days to 40 days. Mechanistic studies revealed that this localized therapy amplifies the ICD cascade through the combined action of DOX and Ca^{2+} overload, which in turn robustly activates dendritic cells and augments the infiltration of cytotoxic T lymphocytes.

Conclusion: This work presents a readily translatable and multifaceted nanomedicine approach that effectively prevents glioma recurrence through synergistic calcium overload and immunomodulation, offering a promising novel strategy for local tumor treatment.

Keywords: Glioma recurrence, $CaCO_3$, Surgiflo, Calcium overload, Immunogenic cell death

Introduction

Glioma is the most common malignant tumor of the central nervous system, characterized by low survival rates, high mortality, and poor prognosis.[1] Its clinical management faces several challenges: (1) Although pharmacotherapy is a primary treatment option, the blood-brain barrier significantly restricts drug selection and therapeutic efficacy;[2] (2) The first-line chemotherapeutic agent temozolomide shows limited efficacy,[3] with drug resistance and systemic toxicity becoming increasingly prominent; (3) Due to the invasive growth pattern of glioma and frequent involvement of functional brain areas, complete surgical resection is often unachievable, leading to high postoperative recurrence

https://doi.org/10.2147/IJN.S578002
Received: 13 November 2025
Accepted: 10 February 2026
Published: 16 February 2026

rates.[4] Clinical observations further indicate that high-grade gliomas almost invariably recur, while low-grade gliomas often progress to higher grades upon recurrence. Currently, there is no standard effective treatment for recurrent glioma, highlighting the urgent need to develop novel therapeutic strategies to prevent recurrence and improve patient outcomes.

Since the 21st century, the rapid advancement of nanomedicine has enabled new approaches for cancer treatment, including targeted therapy and immunotherapy.[5] As drug carriers, nanoparticles can utilize the enhanced permeability and retention (EPR) effect to improve drug accumulation at tumor sites, thereby enhancing anti-tumor efficacy.[6] Additionally, nanocarriers can modulate their interactions with the extracellular matrix to promote drug diffusion and distribution in brain tissue. Several organic nanodrugs have already received clinical approval, such as doxorubicin hydrochloride liposome, amphotericin B liposome, and paclitaxel liposome.[7,8] While these nanodrugs have demonstrated considerable therapeutic efficacy in various other solid malignancies, there remains a notable absence of clinically approved and mature nanomedicines specifically for glioma. In contrast, inorganic nanomaterials have gained increasing research interest due to their simple preparation, unique physicochemical properties, and ease of functional modification.[9] However, their biosafety and clinical translation feasibility remain major challenges.[10] Among various inorganic carriers, calcium carbonate ($CaCO_3$) nanoparticles are considered a highly promising drug delivery system due to their hollow/porous structure, uniform spherical shape, homogeneous particle size, large specific surface area, and acid-responsive degradation.[11] More importantly, $CaCO_3$ primarily consists of calcium, offering good biocompatibility and low in vivo toxicity, and has been approved by the US FDA as a pharmaceutical excipient, demonstrating broad prospects for clinical translation.[12]

$CaCO_3$ nanocarriers can effectively deliver various antitumor drugs, including doxorubicin (DOX), curcumin, cisplatin, and genetic therapeutics.[13–15] As a broad-spectrum anthracycline chemotherapeutic agent, DOX demonstrates significant antitumor efficacy but is limited in clinical application due to severe side effects such as cardiotoxicity and hepatorenal damage.[16] Previous studies have reported that $CaCO_3$-based nano systems co-loading DOX and Fe^{2+} not only markedly inhibit tumor growth but also mitigate the systemic toxicity of DOX, likely by reducing nonspecific systemic exposure through nanocarrier-mediated delivery.[17] Beyond its high drug loading capacity and protective function, $CaCO_3$ enables pH-responsive drug release in the acidic tumor microenvironment, achieving targeted delivery.[6,15,18,19]

Cell membrane-coated nanotechnology has emerged as an important research direction in nanobiomedicine.[20] Tumor cell membranes express specific proteins such as N-cadherin and galectin-3, which confer homologous targeting capability to nanocarriers.[21] By coating nanoparticles with tumor cell membranes, biomimetic drug delivery systems can be constructed that not only retain the EPR effect but also achieve active targeting to homologous tumors through self-recognition mechanisms, thereby improving drug utilization and reducing toxic side effects.[22] Studies have demonstrated that cell membrane-coated nanodrugs exhibit promising antitumor efficacy in targeted therapy.[23,24] Applying this membrane-coating technology to $CaCO_3$ nanocarriers can both enhance their dispersion stability in aqueous solutions and leverage membrane proteins to achieve immune evasion and specific targeting, ultimately improving drug delivery efficiency and therapeutic outcomes.[15,25]

The presence of the blood-brain barrier presents substantial challenges for systemic drug delivery in glioma treatment, with approximately 90% of glioma recurrences occurring within 2 cm of the original resection cavity.[26] Consequently, local drug administration has become an important strategy for preventing postoperative recurrence, as it bypasses the blood-brain barrier, increases local drug concentration at the tumor site, and reduces systemic exposure. However, conventional local drug delivery methods face limitations including restricted drug diffusion, rapid cellular uptake, and uneven distribution, leading to unsatisfactory treatment outcomes.[27] Gliadel wafers, which are carmustine (BCNU)–loaded biodegradable implants, represent an important clinically approved option for local therapy in glioma. Although they have been reported to extend overall survival by approximately 2–4 months, the absolute survival benefit remains modest, and their use is still associated with complications and safety concerns, including pulmonary fibrosis.[28,29]

Since the cavity formed after glioma resection has a three-dimensional structure, conventional local drug administration is prone to drug sedimentation due to gravity, compromising distribution and therapeutic efficacy. The combination of nanomedicines with biological adhesives can effectively improve spatial drug distribution and achieve sustained release. One study developed a degradable phospholipid gel encapsulating temozolomide, which demonstrated sustained

antitumor effects after local application.[30] Using bioadhesives (such as hydrogels) as nanodrug carriers not only optimizes their dispersion but also regulates drug release behavior through gel degradation, thereby enhancing treatment efficacy.[31–33]

Previous studies have demonstrated that $CaCO_3$ nanocarriers loaded with carboplatin and combined with hydrogel can achieve graded drug release through hydrogel degradation and exert antitumor effects when administered locally around subcutaneous tumors.[34] However, the efficacy of such approaches in glioma treatment remains unclear, particularly when applied locally within the postoperative tumor cavity, warranting further investigation. Surgiflo hemostatic gelatin, a sterile absorbable porcine gelatin-based biomaterial widely used for wound hemostasis in neurosurgical and spinal procedures, offers excellent biocompatibility and safety profile, typically being completely absorbed within 4–6 weeks.[35] Utilizing Surgiflo as a nanodrug carrier instead of traditional hydrogels for local administration not only provides postoperative hemostasis but also enables sustained drug release and uniform distribution, showing significant potential for clinical translation.[36]

Based on the aforementioned research background, this study aims to develop a biomimetic targeting system termed CaDM by coating $CaCO_3$ nanocarriers with glioma cell membranes for the delivery of DOX. The antitumor efficacy of CaDM will first be evaluated at the cellular level. Subsequently, the CaDM system will be suspended in Surgiflo bio-gel and administered locally into the postoperative glioma cavity (Scheme 1). The combined CaDM@Surgiflo strategy will be comprehensively assessed for its ability to suppress postoperative glioma recurrence and its underlying mechanisms, with the ultimate goal of providing new therapeutic insights and experimental evidence for clinical application.

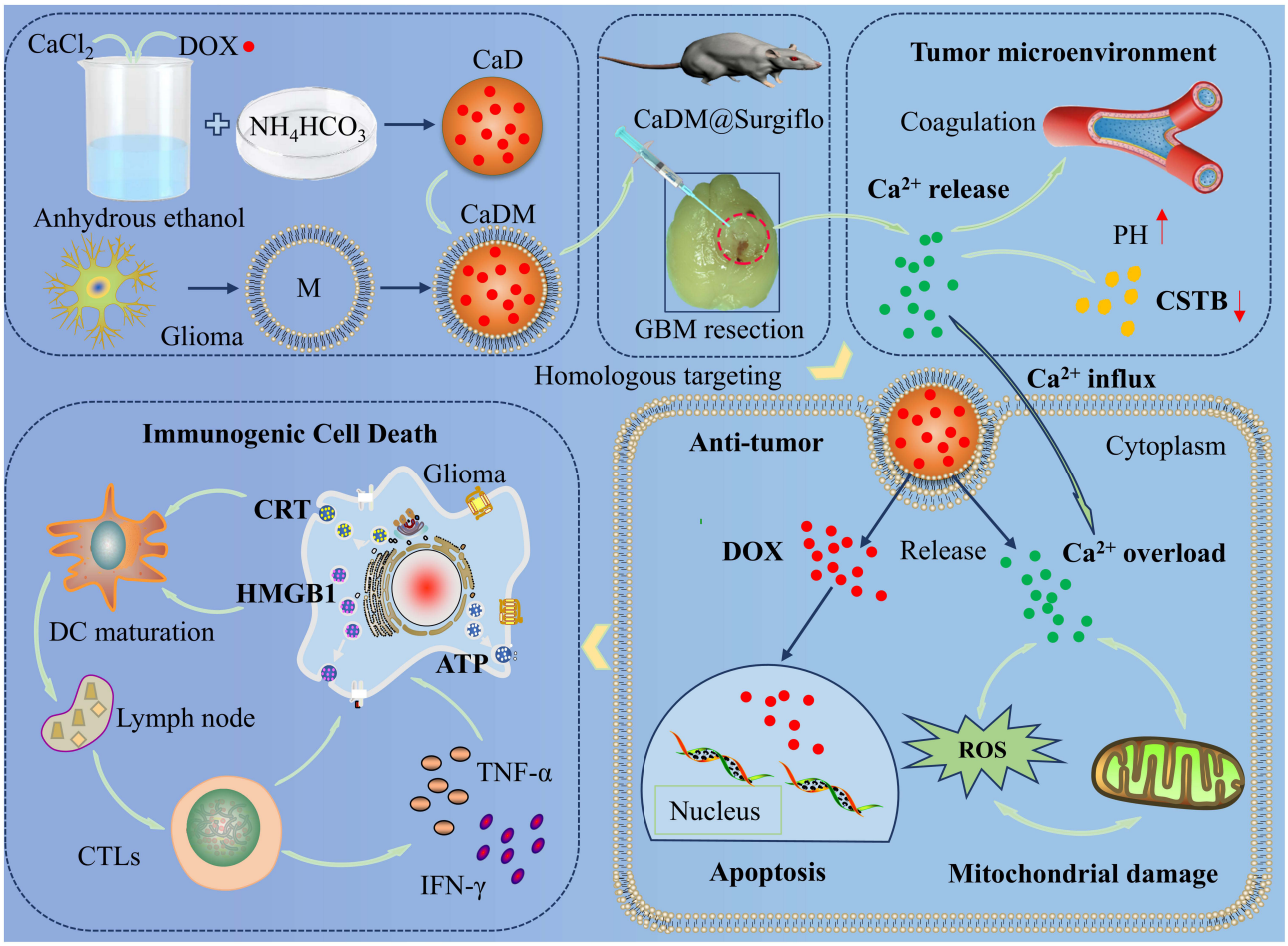

Scheme 1 Schematic illustration of the preparation process and the mechanism of inhibiting glioma recurrence of CaDM@surgiflo. The red dotted circle represents the tumor cavity area after glioma resection, while the upward and downward arrows represent the increase in pH and downregulation of CTSB expression in the tumor microenvironment, respectively.

https://doi.org/10.2147/IJN.S578002

Materials and Methods

Materials

Anhydrous calcium chloride ($CaCl_2$) and ammonium bicarbonate (NH_4HCO_3) were purchased from Tianjin Komiou Chemical Reagent Co., Ltd.; DOX was obtained from Hefei Qiansheng Biotechnology Co., Ltd. Fetal bovine serum, cell culture media, culture dishes, and culture flasks were all sourced from Gibco. Antibodies against CD80, CD86, CRT, HMGB1, CD31, VEGF, Bax, Caspase-3, Ki67, Bcl-2, and PCNA were purchased from Proteintech; antibodies against CD44, CD47, PD-L1, and Na^+/K^+-ATPase were acquired from UpigBio Technology Co., Ltd. CCK-8, ROS, JC-1, Ca^{2+}, live-dead cell staining, mitochondrial membrane potential, and TUNEL apoptosis detection kits, as well as D-luciferin potassium salt, were all supplied by Meilunbio Biotechnology Co., Ltd. (Dalian, China); the ATP assay kit was purchased from Beyotime Biotechnology Co., Ltd.; the Calcium Assay Kit was obtained from Nanjing Jiancheng Bioengineering Institute. Flow cytometry antibodies against CD86, CD80, CD8, CD4, Foxp3, and the HMGB1 detection kit were all procured from Elabscience Biotechnology Co., Ltd. GL261 cells and U251 cells are from the cell bank of the Chinese Academy of Sciences, and C57BL/6 mice are from Shanghai Model Organisms Center, Inc.

Synthesis

$CaCl_2$ (150 mg) and DOX·HCl (4 mg) were dissolved in 100 mL anhydrous ethanol and mixed thoroughly until completely dissolved. The solution was then transferred to a beaker, and the beaker opening was sealed with a transparent microporous film.[17] The sealed beaker was placed together with two Petri dishes containing ammonium bicarbonate (NH_4HCO_3) in a vacuum drying oven at 30°C for 48 h to allow gas-diffusion-mediated mineralization. After the reaction, the precipitate was collected by centrifugation at 10,000 rpm for 30 min and washed three times with anhydrous ethanol to remove residual reagents. The obtained product (CaD) was resuspended in 10 mM HEPES containing 150 mM NaCl (pH 7.2–7.4) to a final concentration of 1 mg/mL. To obtain a homogeneous dispersion, the CaD suspension was subjected to probe sonication. The dispersed CaD suspension was then passed through a 0.45 μm membrane filter, and the filtrate was collected for subsequent cell-membrane coating. CaNP was prepared using the same gas diffusion method, except that DOX was not added.

Glioma cell lines GL261 and U251 MG were harvested and resuspended in ice-cold buffer (10 mM HEPES, 150 mM NaCl, pH 7.2–7.4) supplemented with protease inhibitors, and all procedures were performed on ice. Cells were disrupted by 3–5 freeze–thaw cycles (liquid nitrogen freezing followed by thawing at room temperature). The lysate was centrifuged at 800–1,000 g for 10 min to remove nuclei and large debris, and the supernatant was collected and further centrifuged at 20,000 g for 30 min to pellet the membrane fraction. The membrane pellet was resuspended in buffer and washed 1–2 times by centrifugation at 20,000 g for 30 min to remove soluble proteins. The final membrane pellet was resuspended in buffer to prepare membrane vesicles, and the membrane protein concentration was adjusted to 1,000 μg/mL. The membrane vesicles were further homogenized by intermittent water-bath sonication on ice (42 kHz; 30–60 s × 2–3 cycles with cooling intervals). Subsequently, an equal volume of membrane vesicle suspension was slowly added dropwise to the CaD suspension, followed by gentle inversion or low-speed vortexing for 5–10 s. The mixture was then subjected to intermittent water-bath sonication (42 kHz) on ice (30–60 s × 3 cycles) to facilitate membrane coating, yielding CaDM. Finally, the CaDM suspension was filtered through a 0.45 μm membrane to remove trace aggregates, and the filtrate was collected as the final CaDM formulation. The as-prepared CaDM was stored at 4°C and used for subsequent cell-based experiments within 24 h to preserve the immunogenic activity of the membrane proteins.

Characterization

The morphology and size of nanoparticles were examined using transmission electron microscopy (TEM). Elemental composition and content were analyzed by energy-dispersive X-ray spectroscopy (EDS). The hydrodynamic diameter and zeta potential were measured with a particle size analyzer. Absorption spectra and fluorescence properties were characterized using ultraviolet and fluorescence spectrophotometers, respectively. Qualitative and quantitative detection of cell membrane proteins coated on the nanoparticle surface was performed through SDS-PAGE (Coomasie blue staining, details shown in Supplementary Methods 1) and Western blot analysis (details shown in Supplementary Methods 2).

pH-Responsive Release Study

CaDM samples were placed in dialysis bags and immersed in PBS buffers at pH 5.5, 6.5, and 7.4. The release experiment was conducted in a light-proof shaking incubator at 37°C with constant shaking at 200 rpm. At predetermined time points, equal volumes of release medium were collected from each group. The DOX content in the medium was measured using a fluorescence spectrophotometer, and the cumulative release rate was calculated based on a standard curve to plot drug release kinetics. Simultaneously, Ca^{2+} concentration in the release medium at each time point was determined using a Calcium Assay Kit, and corresponding Ca^{2+} release curves were generated. To further observe structural changes of the material under different pH conditions, CaDM was treated in the aforementioned PBS buffers at three pH levels for 0.5 hour, followed by morphological and structural examination using TEM.

Cellular Uptake and Targeting Evaluation

U251 MG glioma cells and HA1800 normal astrocytes were seeded in 24-well plates at a density of 2×10^4 cells per well. After 24 hours of culture, CaDM (100 μg/mL) was added and incubated with the cells for 2 hours. The targeting ability of CaDM toward glioma cells was then assessed using fluorescence microscopy and flow cytometry, with intracellular DOX distribution and content analyzed simultaneously.

In a separate experiment, U251 MG cells were cultured in 24-well plates and treated with CaDM (100 μg/mL). At different time points post-incubation, cellular uptake of CaDM was examined using fluorescence microscopy and flow cytometry, allowing quantitative analysis of the dynamics of DOX internalization.

In vitro Antitumor Activity Assay

GL261 glioma cells were seeded in 96-well plates at 5×10^3 cells per well. After 24 hours of culture, cells were treated with CaNP, CaD, or CaDM for 8 hours, followed by continued incubation until 24 hours. Cell viability was then measured using the CCK-8 assay by detecting absorbance at 450 nm. In a separate experiment, cells were treated with CaDM for 8 hours in media at pH 7.4 or pH 6.5, and cell viability was similarly assessed using the CCK-8 assay. Additionally, under both pH 7.4 and pH 6.5 conditions, cells were treated with CaNP, CaD, or CaDM at a concentration of 20 μg/mL for 24 hours, stained with AM/PI live-dead cell double-staining kit, and observed under a fluorescence microscope to evaluate cell survival and death.

Detection of Ca^{2+}, ROS, Mitochondrial Membrane Potential, and Mitochondrial Morphology

GL261 glioma cells were seeded in 24-well plates at approximately 2×10^4 cells per well. After 24 hours of culture, the cells were treated with CaNP, CaD, or CaDM at a concentration of 20 μg/mL for 8 hours. The following assays were then performed:

Ca^{2+} Detection

Cells were incubated with 3 μM Fluo-4 AM working solution at 37°C for 30 min, followed by replacement with HBSS buffer and further incubation for 30 min (details shown in Supplementary Methods 3). Ca^{2+} distribution and fluorescence intensity were observed under a fluorescence microscope (excitation wavelength: 494 nm).

ROS Detection

Cells were incubated with 10 μM DCFH-DA working solution at 37°C for 30 min, washed three times with serum-free culture medium, and ROS distribution and fluorescence intensity were observed under a fluorescence microscope (excitation wavelength: 488 nm).

Mitochondrial Membrane Potential Detection

Cells were incubated with JC-1 staining working solution at 37°C for 20 min. After removing the supernatant and washing three times with buffer, fresh culture medium was added. Fluorescence distribution of JC-1 monomers

(excitation wavelength: 490 nm) and aggregates (excitation wavelength: 525 nm) was observed under a fluorescence microscope (details shown in Supplementary Methods 4).

Mitochondrial Morphology Detection

Cells were incubated with 100 nM MitoTracker® Green FM staining working solution at 37°C for 30 min, followed by replacement with fresh culture medium (details shown in Supplementary Methods 5). Mitochondrial distribution and fluorescence intensity were observed under a fluorescence microscope.

Detection of Immunogenic Cell Death (ICD) Markers

GL261 glioma cells were seeded in 24-well plates at approximately 2×10^4 cells per well. After 24 hours of culture, cells were treated with CaNP, CaD, or CaDM with a concentration of 20 μg/mL for 4 hours, and then incubated for 24 hours.

Immunofluorescence Assay

Cells were fixed with 4% paraformaldehyde and blocked with 5% BSA. Primary antibodies against CRT and HMGB1 were added and incubated overnight at 4°C. After washing three times with PBS, corresponding fluorescent secondary antibodies were applied and incubated for 2 hours at room temperature. Nuclei were stained with DAPI for 3 minutes, followed by additional PBS washes. The cells were mounted with anti-fade mounting medium and observed under a fluorescence microscope to examine the localization and expression intensity of CRT and HMGB1.

Western Blot Analysis

Parallel samples treated identically were collected for total protein extraction. CRT and HMGB1 protein expression levels were detected by Western blot (details shown in Supplementary Methods 2).

Detection of Cell Supernatant

GL261 cells were seeded in 6-well plates at approximately 10×10^4 cells per well. After 24 hours of culture, cells were treated with CaNP, CaD, or CaDM for 4 hours, followed by continued incubation until 24 hours. Cell culture supernatants were then collected, and extracellular ATP release and HMGB1 levels were measured using an ATP assay kit and HMGB1 ELISA kit, respectively.

Orthotopic Glioma Model Establishment and Postoperative Local Treatment

GL261-LUC glioma cells stably expressing firefly luciferase were cultured and collected at 80–90% confluence, washed once with PBS, and resuspended for subsequent use. C57BL/6 mice were anesthetized with isoflurane and secured in a stereotactic frame. Isoflurane anesthesia was administered via a precision vaporizer, with an induction dose of 3–4% and a maintenance dose of 1.5–2% in oxygen. After shaving and disinfecting the scalp, a midline incision was made. A 1 mm burr hole was drilled using a dental drill at a position 2.0 mm right and 0.5 mm posterior to the bregma. A microsyringe was used to draw the cell suspension, which was then injected vertically to a depth of 3 mm before retracting 1 mm. The injection was performed slowly at a rate of 1 μL/min, followed by a 5-minute waiting period before slow needle withdrawal. The number of tumor cells injected into each mouse is 2×10^5, and the injection volume is 5 μL. The burr hole was sealed with bone wax, the skin incision was sutured, and antibiotics were administered postoperatively to prevent infection.

Following tumor inoculation, establishment was verified via in vivo fluorescence imaging at the one-week time point. Mice confirmed to be tumor-bearing were then anesthetized and positioned in a stereotaxic frame. The prior surgical incision was reopened to access the skull, and the burr hole was carefully enlarged using a hand-held drill to achieve complete exposure of the tumor mass. Subtotal resection of the glioma was performed under microscopic guidance, with bipolar electrocautery used for hemostasis during the procedure. A mixture of 5 mg CaDM dispersed in 1 mL of normal saline and 2 mL of Surgiflo fluid gelatin was prepared and injected into the tumor cavity for local administration, with approximately 20 μL administered per mouse. After the procedure, the skull was routinely closed, and the scalp was sutured. Penicillin was administered daily via intramuscular injection to prevent infection. The general condition of the mice was monitored regularly, and body weight changes and survival time were recorded. At

the experimental endpoint, mice were euthanized by CO_2 inhalation followed by cervical dislocation, which is consistent with the AVMA Guidelines for Euthanasia of Animals. All experimental mice were housed and managed in strict accordance with institutional guidelines, and the study was approved by the Animal Ethics Committee of Anhui Medical University (LLSC20241641).

In vivo Antitumor Efficacy and Mechanism Evaluation

A D-luciferin potassium salt solution (30 mg/mL) was prepared in D-PBS and administered to mice via intraperitoneal injection at a dose of 0.15 mg/g. Bioluminescence imaging was initiated 5–10 minutes post-injection, and tumor recurrence was monitored weekly at weeks 1, 2, 3, and 4 using an in vivo fluorescence imaging system.

Four weeks after local treatment, all mice were euthanized. Major organs and brain tissues were collected, fixed in 4% paraformaldehyde, embedded in paraffin, and sectioned. The sections were subjected to HE staining, IHC staining for CRT, HMGB1, CD31, VEGF, Bax, Caspase-3, Ki67, Bcl-2, and PCNA, TUNEL apoptosis assay, and Masson staining (details shown in Supplementary Methods 6 and 7).

Additionally, brain tumor tissues were accurately weighed and homogenized in deionized water at a 1:9 (g/mL) ratio in an ice bath. The homogenate was centrifuged at 2500 rpm for 10 minutes, and 10% of the supernatant was collected. Ca^{2+} content in the tumor tissue was measured using a calcium assay kit.

Safety Evaluation

Mice bearing orthotopic gliomas were anesthetized, and gentle pressure was applied to both sides of the neck while pulling the skin backward to promote congestion of the retro-orbital venous plexus. A capillary blood collection tube was inserted from the medial canthus and advanced at a 30–45° angle to the nasal plane along the inner canthus. The tube was gently rotated to puncture the venous plexus and collect blood. After collection, pressure on the mouse was released to allow the eyeball to return to its natural position. The capillary tube was slowly withdrawn, and a dry cotton ball was applied to the orbit to achieve hemostasis. Whole blood samples were collected to measure serum levels of ALT, AST, BUN, WBC, HGB, RBC, and Ca^{2+}.

At the end of the experiment, mice were euthanized, and tissues including the brain, heart, liver, spleen, lungs, and kidneys were collected. These tissues were embedded in paraffin, sectioned, and stained with H&E for morphological observation under a light microscope.

Detection of ICD and Related Immune Cells

In vitro experiments: Bone marrow-derived dendritic cells (BMDCs) were isolated and cultured from 8-week-old C57BL/6 mice (37399132). These BMDCs were then co-cultured for 24 hours with GL261 cells that had been pre-treated for 12 hours under different conditions. The GL261 cells were divided into four treatment groups: PBS (control), CaNP, CaD, and CaDM. After co-culture, BMDCs were collected, washed three times with PBS, and stained in the dark for 30 minutes with the following flow cytometry antibodies: anti-CD11c-APC, anti-CD80-PE, and anti-CD86-FITC. After washing, the expression levels of CD80 and CD86 were analyzed by flow cytometry.

In vivo experiments: Brain tissue from locally treated tumor-bearing mice was collected, rinsed three times with sterile PBS, minced, and digested with type IV collagenase to prepare a single-cell suspension. The suspension was sequentially filtered through 80-mesh and 200-mesh cell strainers. The following antibody combinations were used for staining: anti-CD3-FITC, anti-CD4-PE, and anti-CD8-APC to identify $CD3^+CD4^+$ and $CD3^+CD8^+$ T cell subsets; anti-CD25-APC, anti-CD4-PE, and anti-Foxp3-FITC to identify $CD4^+Foxp3^+$ regulatory T cells (Tregs). Dendritic cells (DCs) were detected using the same method as in the in vitro experiments. Additionally, part of the brain tissue was used for immunofluorescence staining to observe the spatial expression and distribution of CD80 and CD86 proteins (details shown in Supplementary Methods 7).

Statistical Analysis

All quantitative data are expressed as mean ± standard deviation (SD). Statistical analyses were conducted with GraphPad Prism (version 9.0). Intergroup differences were evaluated by an unpaired Student's *t*-test (two groups) or one-

way ANOVA followed by a suitable post-hoc test (multiple groups). The Log-rank (Mantel–Cox) test was applied to analyze survival data. Differences with a *P*-value below 0.05 were considered statistically significant, and significance levels were designated as follows: *P < 0.05, **P < 0.01, ***P < 0.001, and ****P < 0.0001.

Results and Discussion

Preparation and Characterization of CaDM

The preparation process of CaDM is illustrated in Figure 1A. Using an established one-pot gas diffusion method,[37] doxorubicin (DOX)-loaded $CaCO_3$ nanoparticles (CaD) were first synthesized. Subsequently, glioma cell membranes were extracted and coated onto the surface of CaD to obtain CaDM. Based on a standard curve, the drug loading efficiency of DOX was calculated to be 9.7%.

TEM results confirmed the successful construction of CaNP, CaD, and CaDM, with relatively uniform particle distribution (Figures 1B and S1). The particle size of CaDM was approximately 100 nm, and the thickness of the coated

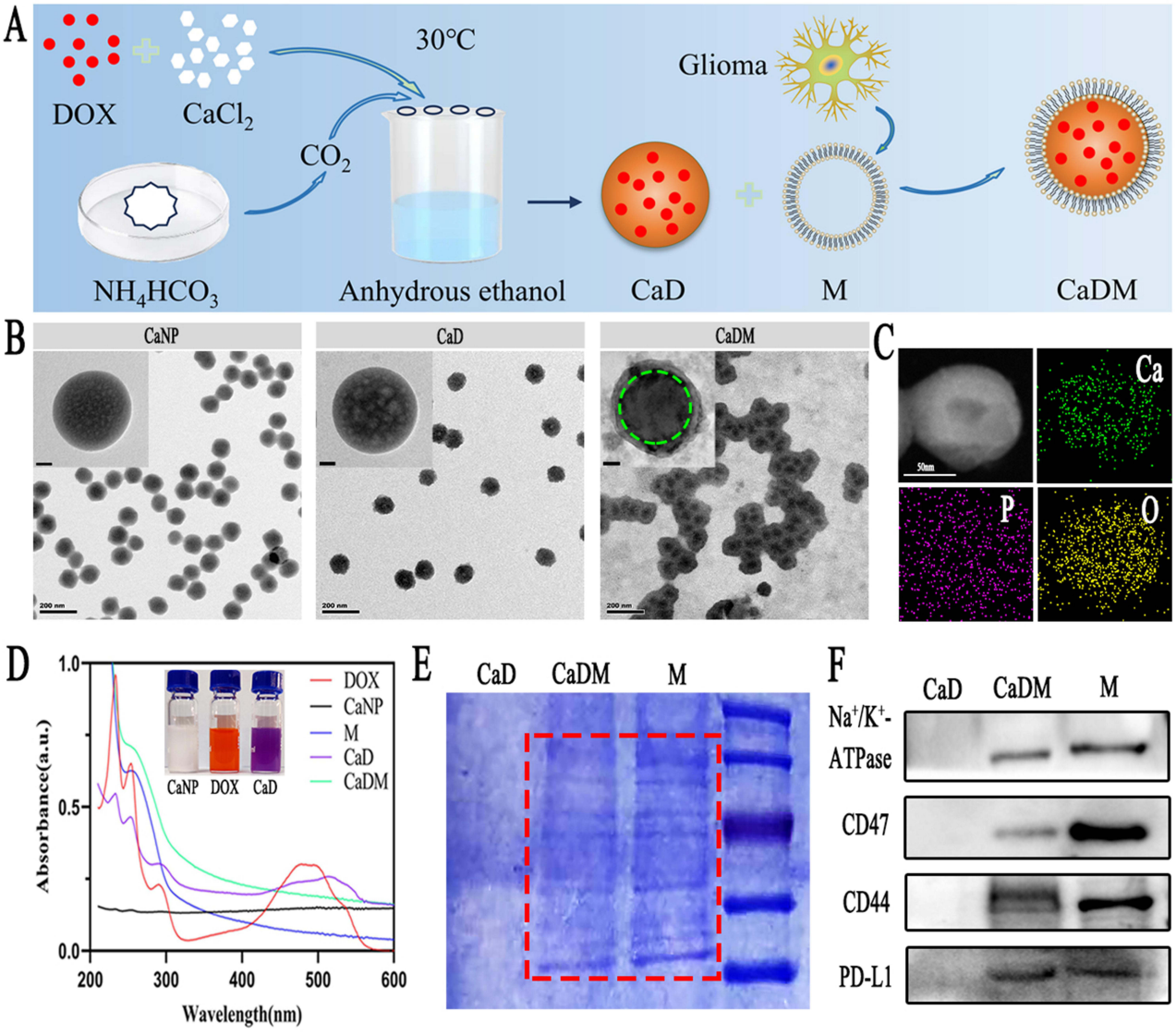

Figure 1 Characterization of the CaDM. (**A**) Schematic diagram of CaDM synthesis. (**B**) TEM images of CaNP, CaD, and CaDM. (**C**) EDS element mapping images of CaDM. (**D**) UV-vis spectra of DOX, CaNP, CaD, M, and CaDM. (**E**) Coomassie Brilliant Blue staining of GL261 cell membrane proteins based on SDS-PAGE. (**F**) Western blot detection of surface membrane protein on GL261 cell. The green circle represents CaD, and the red box is the main characteristic protein band of the cell membrane. Enlarged TEM image; scale bar = 20 nm.

cell membrane was about 10 nm, consistent with previous reports.[15] Studies have shown that nanoparticles in the size range of 50–200 nm are more likely to achieve efficient passive targeting in solid tumors, exhibit better retention in tumor tissues, and undergo lower clearance. After entering tumor tissues, especially in areas beyond vascular reach, their penetration depth is negatively correlated with particle size.

Zeta potential analysis showed that the surface potential became more negative after membrane coating, indicating successful attachment of the cell membrane onto the $CaCO_3$ nanoparticle surface. Specifically, the zeta potential shifted from −9.95 mV before coating to −17.89 mV after membrane encapsulation (Figure S2). Due to the inherent hydrophilic nature of the material, the hydrodynamic diameter measured by DLS was slightly larger than that observed by TEM, though both showed consistent trends (Figure S3). EDS elemental mapping and spectrum analysis further confirmed the presence and uniform distribution of Ca, P, and O elements (Figures 1C, S4, and S5).

UV-Vis spectroscopy showed that the characteristic absorption peak of DOX was retained, with a red shift observed, indicating successful drug loading within the nanostructure (Figure 1D). The color of the solution changed from orange to purple after synthesis, consistent with observations in other studies.[37] Meanwhile, fluorescence absorption spectra revealed characteristic absorption peaks of DOX, and their intensity increased with concentration (Figure S6). Additionally, both Coomassie blue staining and Western blot confirmed the retention of characteristic cell membrane proteins, demonstrating successful membrane coating (Figure 1E and F).

Acid-Responsive Release and Homologous Targeting of CaDM in vitro

$CaCO_3$ nanoparticles exhibit excellent acid-responsive release properties, which are highly significant for the weakly acidic tumor microenvironment. As shown in Figure 2A, TEM observations under different pH conditions revealed that the degradation of nanoparticles significantly intensified as the pH decreased. Analysis of DOX release behavior further confirmed this characteristic: in an acidic environment (pH 5.5), both the release rate and cumulative release of DOX were significantly higher than under neutral conditions (Figure 2B). Similarly, Ca^{2+} release experiments showed a consistent trend, collectively demonstrating the favorable pH-responsive release capability of CaDM (Figure S7).

Studies have indicated that cell membrane-coated nanoparticles can significantly enhance uptake efficiency by homologous tumor cells compared to uncoated nanoparticles. To verify the homologous targeting ability of CaDM, in vitro cellular uptake experiments were conducted. As shown in Figure 2C, stronger DOX fluorescence signals were detected in U251 MG glioma cells compared to normal HA1800 astrocytes. Quantitative flow cytometry analysis further confirmed that the uptake of CaDM by U251 MG cells was significantly higher than CaD (Figure 2D), indicating the excellent homologous targeting of CaDM toward glioma cells. Uptake kinetics experiments demonstrated that intracellular DOX content gradually increased with incubation time and plateaued after 2 hours (Figure 2E and F).

CCK-8 assays revealed that CaDM more effectively inhibited glioma cell proliferation compared to other groups, with its antitumor effect being more pronounced in an acidic microenvironment (Figure 2G). Live-dead cell staining further confirmed that CaDM induced a higher proportion of tumor cell death in vitro (Figure 2H). Based on the CCK-8 and AM/PI assays, CaDM exhibited an inhibitory effect on cell viability at a concentration of 20 μg/mL. Notably, its antitumor activity was significantly enhanced when the incubation time was prolonged and/or the pH was lowered. This can be attributed to the accelerated release of Ca^{2+} and DOX from CaDM under acidic conditions, resulting in a synergistic enhancement of tumor cell killing.

In vivo Antitumor Efficacy of CaDM@Surgiflo

After preoperative assessments to confirm tumor establishment and determine tumor burden in the orthotopic glioma–bearing mice (Figures S8 and S9), subtotal tumor resection was performed, followed by local administration into the resection cavity (Figure 3A). The fluid gelatin Surgiflo, functioning as a biological adhesive, not only achieved effective hemostasis but also promoted uniform distribution and spatial retention of CaDM within the cavity (Figure 3B and C). Postoperative in vivo fluorescence imaging was used to select mice with satisfactory surgical outcomes, and tumor recurrence was monitored at various time points (Figure 3D), alongside recording body weight changes and survival status.

https://doi.org/10.2147/IJN.S578002

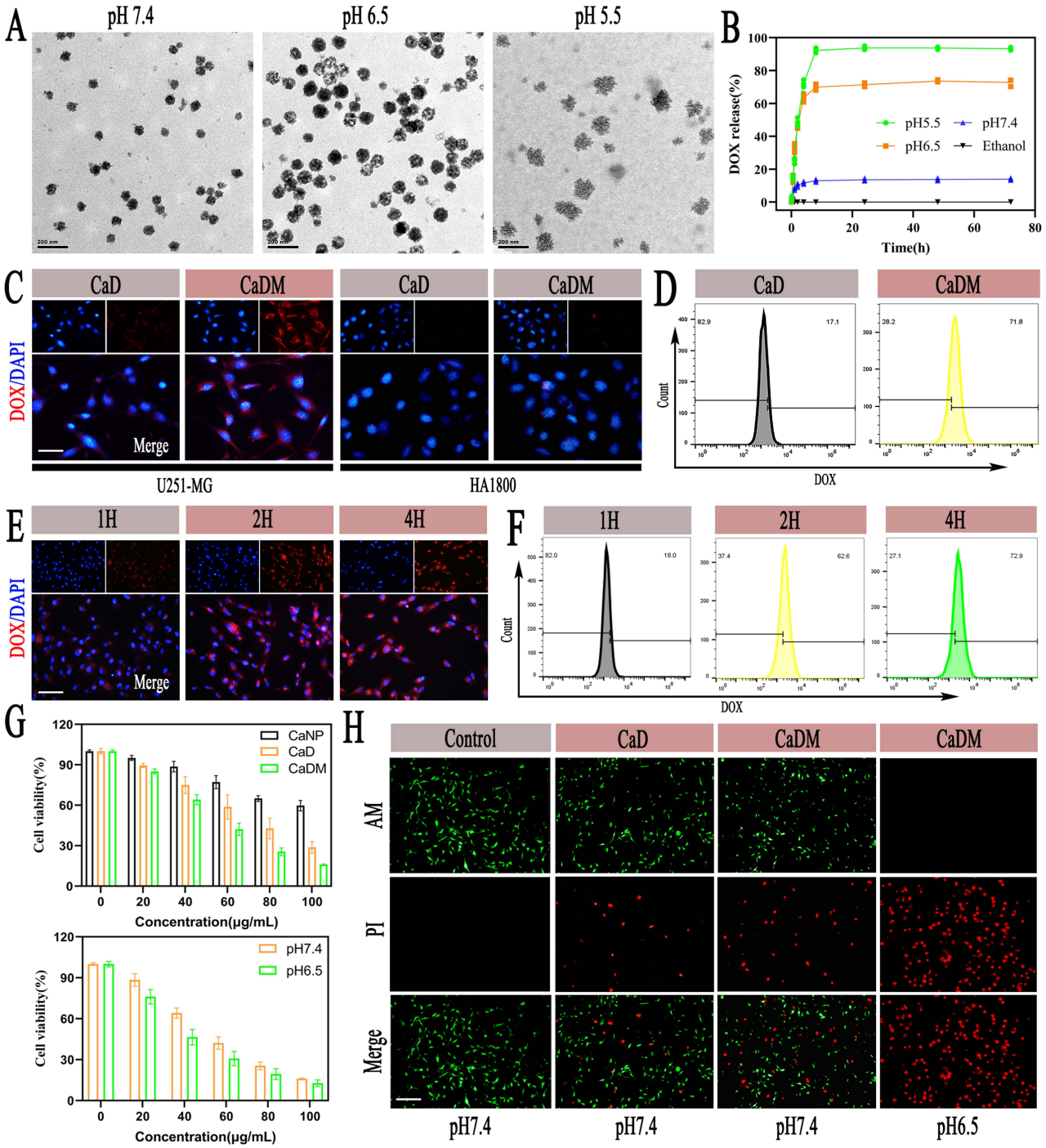

Figure 2 Extracellular acid release properties and in vitro anti-tumor ability of CaDM. (**A**) TEM images of CaDM in pH 7.4, 6.5, and 5.5. (**B**) Release of DOX from CaDM in PH 7.4, 6.5, and 5.5. (**C**) Fluorescence images of DOX phagocytosis in U251-MG and HA1800 cells. Scale bar is 20μm. (**D**) Detection of DOX phagocytosis in GL261 cells by flow cytometry. (**E**) Fluorescence images of DOX phagocytosis in GL261 cells at 1H, 2H, and 4H. Scale bar is 50μm. (**F**) Detection of DOX phagocytosis in GL261 cells at different times by flow cytometry. (**G**) The cell viability of GL261 cells treated with CaNP, CaD, and CaDM in pH 7.4 and 6.5. (**H**) Fluorescence images of GL261 cells stained with calcein AM-PI. Scale bar is 100μm.

The CaDM@Surgiflo group showed marked suppression of tumor growth (Figure 3E) and prolonged the median survival from 14 to 40 days, with reduced body-weight loss relative to the control groups (Figures 3F and G). The therapeutic efficacy was visually represented using distinct colors for each group (Figure 3H). Histopathological analysis by H&E staining confirmed these findings, showing smaller tumor mass and looser cell arrangement in the CaDM@Surgiflo

https://doi.org/10.2147/IJN.S578002

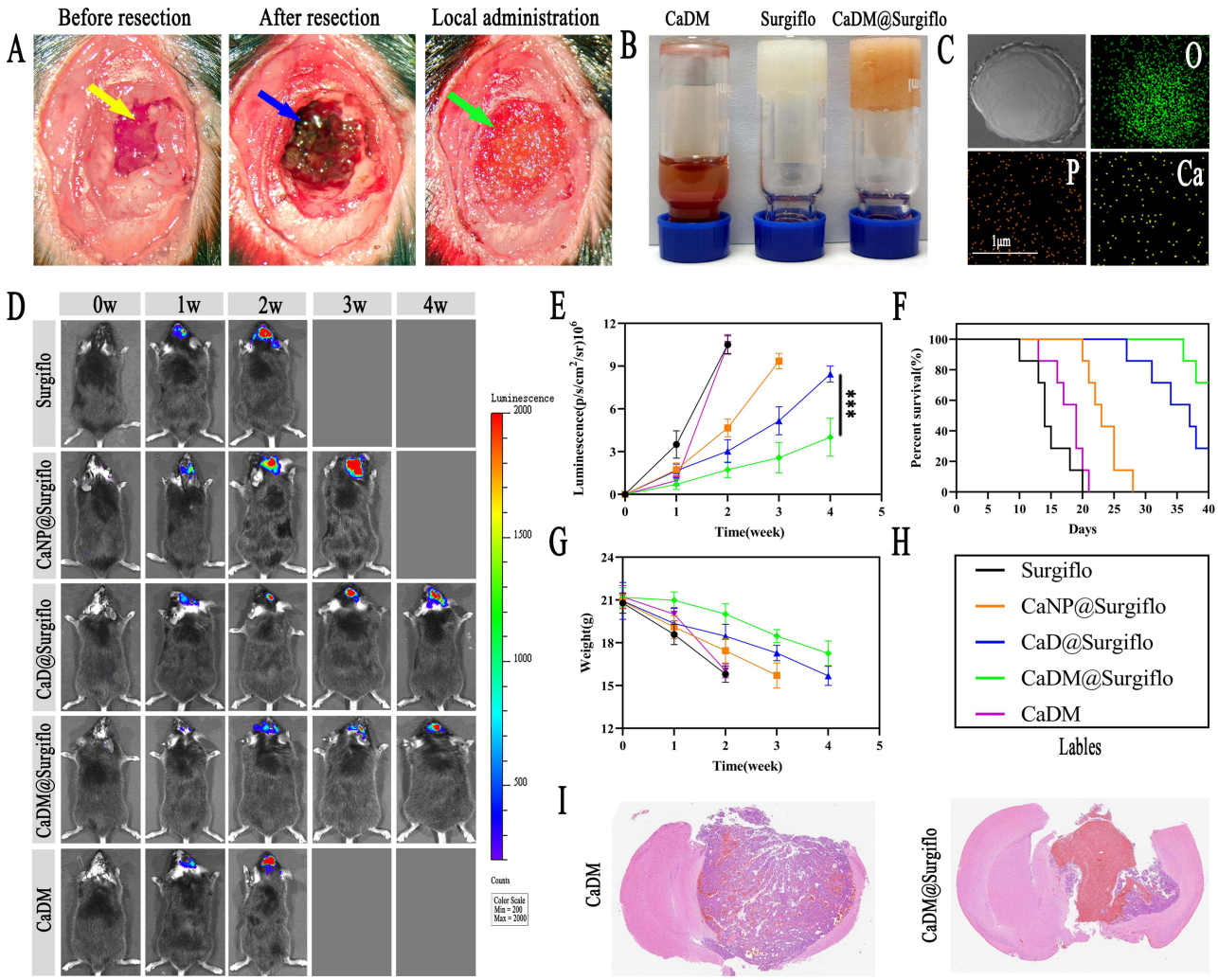

Figure 3 Inhibition of tumor recurrence by CaDM@Surgiflo through local delivery after glioma resection. (**A**) Tumor resection and postoperative in situ administration in glioma-bearing mice. Yellow arrow: formed tumor. Blue arrow: Cavity after tumor resection. Green arrow: CaDM@Surgiflo in situ administration. (**B**) Representative photographs showing the gross appearance and morphology of CaDM, Surgiflo, and CaDM@Surgiflo. (**C**) STEM images of CaDM@Surgiflo and the corresponding element mapping. (**D**) In vivo bioluminescence images of glioma-bearing mice after in situ administration, and (**E**) Semi-quantitative statistical analysis. (**F**) Survival curves and (**G**) body weight changes of glioma-bearing mice in each group. (**H**) Groups represented by different colors. (**I**) H&E stained-images of brain sections from CaDM and CaDM@Surgiflo groups. ***P < 0.001.

group, in contrast to the dense cellular architecture indicative of recurrence in other groups (Figure 3I and S10). These outcomes are attributed to the dual targeting mechanism of the biomimetic nanoparticles: passive accumulation in the tumor tissue via the EPR effect, followed by active internalization into glioma cells through homologous binding mediated by the cancer cell membrane coating.

To further evaluate the antitumor efficacy of CaDM@Surgiflo in vivo, IHC and TUNEL staining were performed. IHC results indicated significant upregulation of the pro-apoptotic proteins Bax and Caspase-3 in tumor tissues of the CaDM@Surgiflo group (Figure 4A–D), while expression of the anti-apoptotic protein Bcl-2 and proliferation markers Ki67 and PCNA were notably reduced (Figures S11 and S12). TUNEL assays further confirmed that the apoptosis rate of tumor cells in this treatment group was significantly higher than in other groups (Figure 4E).

Additionally, H&E staining showed no significant pathological damage in major organs such as the heart, liver, spleen, lungs, and kidneys of mice across all groups (Figure S13). Routine blood tests and biochemical indicators (including Ca^{2+} levels) were within normal ranges (Figures S14 and S15), indicating favorable biosafety of the local delivery strategy based on $CaCO_3$ nanocarriers.

https://doi.org/10.2147/IJN.S578002

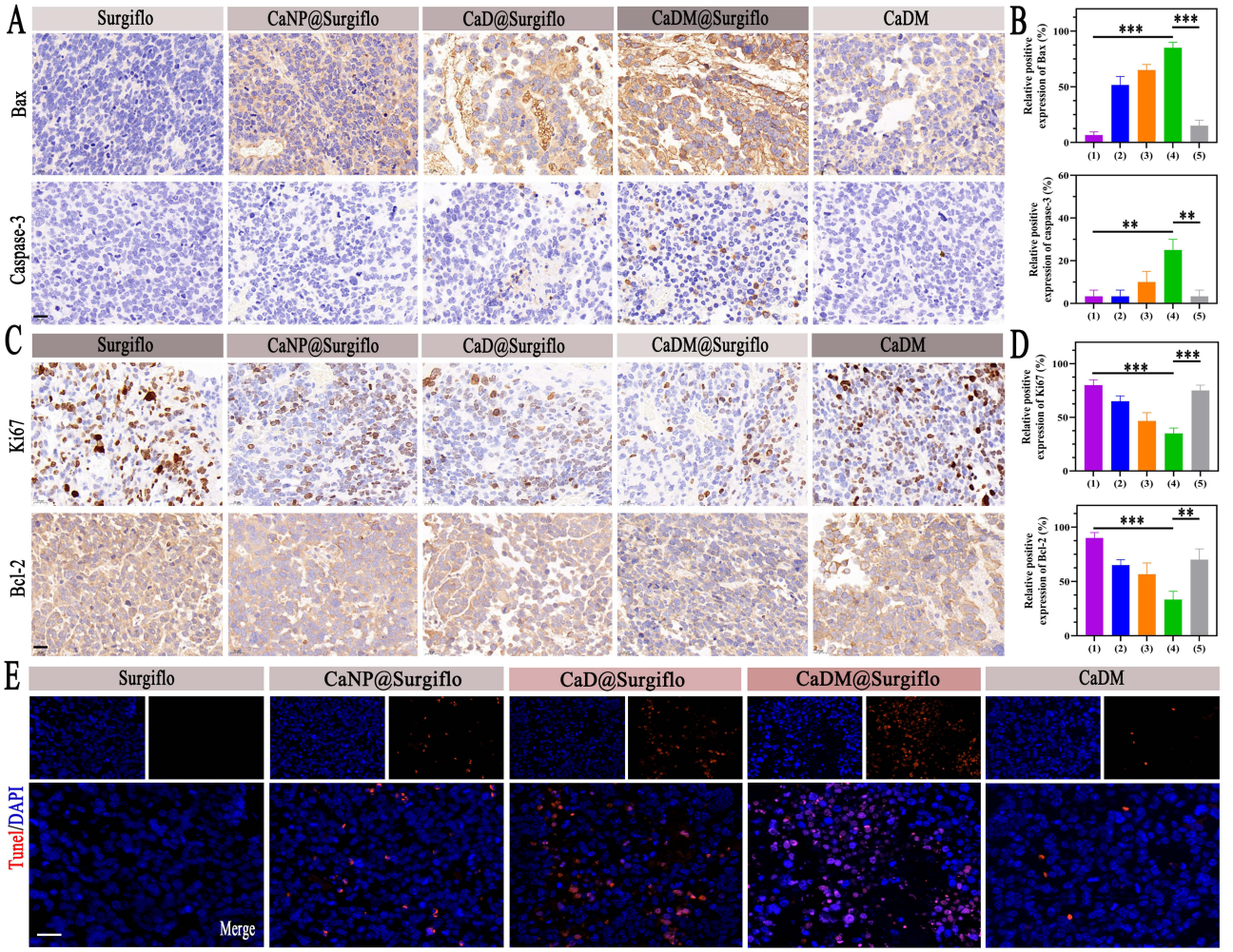

Figure 4 In vivo anti-tumor ability of CaDM@Surgiflo. (**A**) Immunohistochemical-stained images of Bax and Caspase-3, and (**B**) Semi-quantitative statistical analysis in tumor tissues of various groups. Scale bar is 20μm. (**C**) Immunohistochemical-stained images of Bax and Caspase-3, and (**D**) Semi-quantitative statistical analysis in tumor tissues of various groups. Scale bar is 20μm. (**E**) Tunel-stained images of tumor tissues from various groups. Scale bar is 20μm. (1) Surgiflo, (2) CaNP@ Surgiflo, (3) CaD@ Surgiflo, (4) CaDM@ Surgiflo, (5) CaDM. **P < 0.01, and ***P < 0.001.

Antitumor Mechanism of CaDM in vitro

Upon internalization by glioma cells via homologous targeting, CaDM rapidly degrades in the acidic intracellular environment, releasing substantial amounts of Ca^{2+} and DOX. To investigate its antitumor mechanism, we focused on calcium overload and the resulting mitochondrial damage. As shown in Figure 5A and B, the CaDM-treated group exhibited significantly higher intracellular Ca^{2+} fluorescence intensity compared to other groups, accompanied by a marked increase in ROS levels, indicating that calcium overload triggered intense oxidative stress.

Assessment of mitochondrial membrane potential using the JC-1 probe revealed a significant enhancement of green fluorescence (indicating loss of membrane potential) and a notable reduction in red fluorescence (indicating normal membrane potential) in the CaDM group, suggesting severe impairment of mitochondrial function (Figure 5C). Furthermore, MitoTracker® Green FM staining showed a significant decrease in mitochondrial number in the CaDM group, further confirming disruption of mitochondrial structural integrity (Figure 5D).

As a known inducer of ICD, DOX promotes the release of various damage-associated molecular patterns (DAMPs), including CRT exposure, ATP secretion, and HSP70 and HMGB1 release. This study found that CaDM treatment not only induced ICD via the DOX pathway but also enhanced this effect through ROS accumulation triggered by calcium overload. Immunofluorescence results showed significantly upregulated CRT expression on the cell membrane and increased HMGB1 release from the nucleus in the CaDM group (Figure 6A and B), a trend further validated by

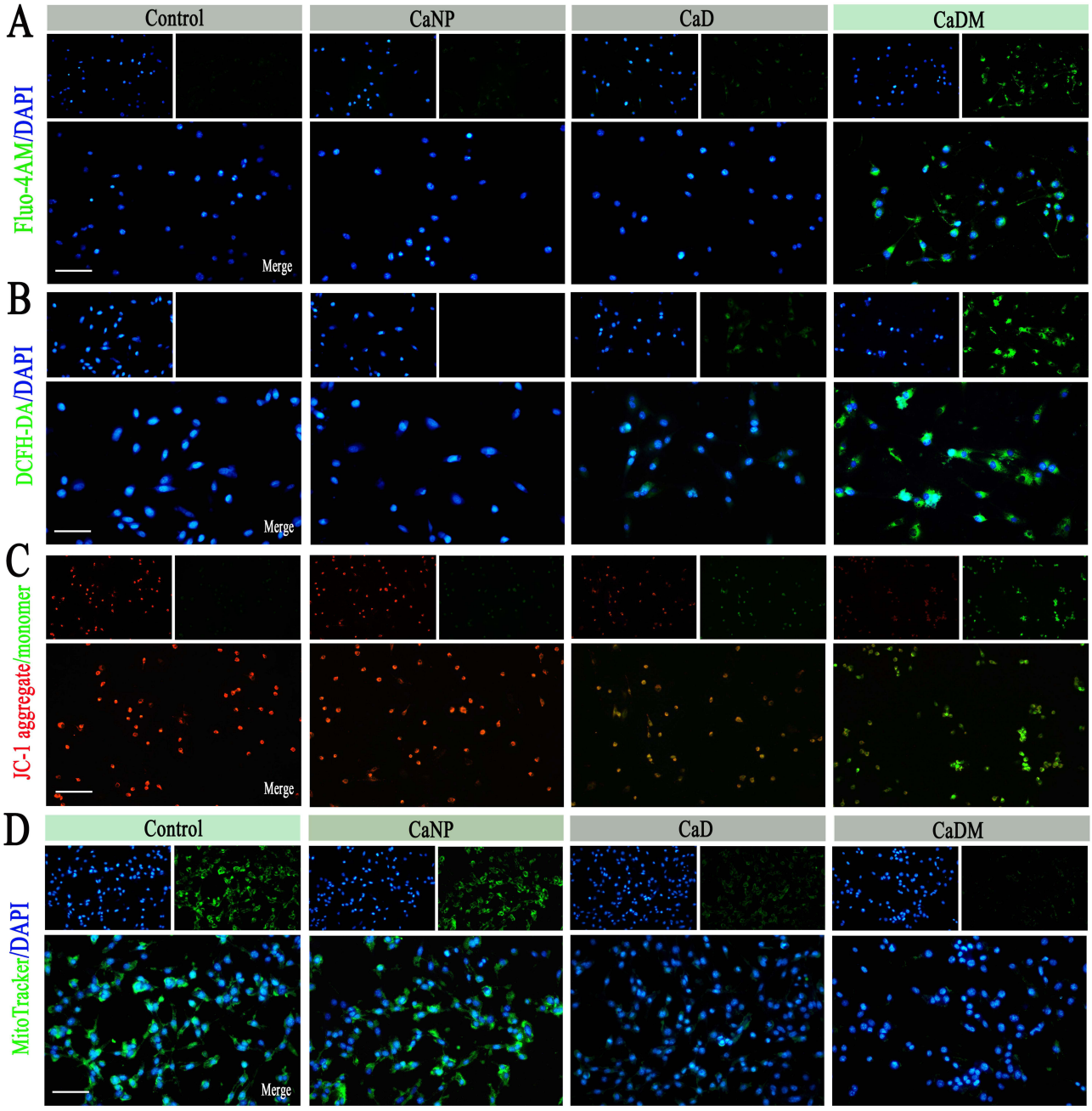

Figure 5 Mitochondrial calcium overloaded triggers ROS in vitro. (**A**) Detection of Ca^{2+} in various groups. Scale bar is 100μm. (**B**) Detection of ROS in various groups. Scale bar is 50μm. (**C**) Detection of mitochondrial membrane potential in various groups. Scale bar is 100μm. (**D**) Detection of mitochondrial distribution in various groups. Scale bar is 100μm.

Western blot analysis (Figure 6C and D). Concurrently, the secretion levels of ATP and HMGB1 in the culture medium were significantly elevated after CaDM treatment (Figure 6E and F).

To further evaluate whether CaDM could promote DCs maturation through ICD induction, a Transwell co-culture system was employed. As shown in Figure 6G and H, glioma cells treated with CaDM in the upper chamber significantly promoted the maturation of BMDCs in the lower chamber. These results collectively demonstrate that CaDM effectively induces ICD in glioma cells in vitro, thereby activating an antitumor immune response.

https://doi.org/10.2147/IJN.S578002

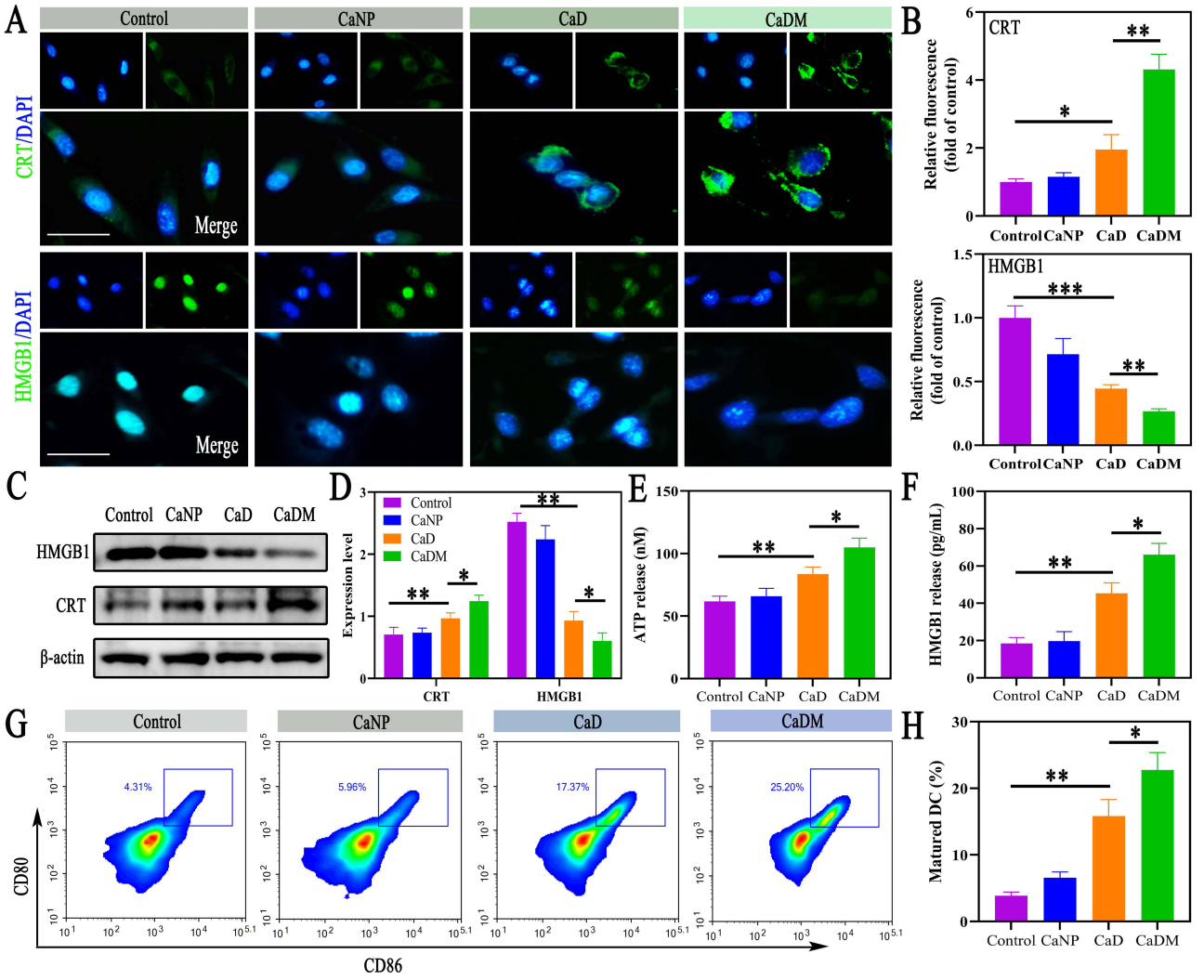

Figure 6 Activation of ICD by CaDM in vitro. (**A**) Fluorescence images of CRT and HMGB1, and (**B**) Semi-quantitative statistical analysis in GL261 cells. Scale bar is 20μm. (**C**) Western blot analysis of ATP and HMGB1, and (**D**) Semi-quantitative statistical analysis in various groups. (**E**) ATP and (**F**) HMGB1 released from GL261 cells in various groups. (**G**) Flow cytometry analysis of CD80 and CD86 for DC maturation, and (**H**) Semi-quantitative statistical analysis in various groups. The blue box denotes cells that are double-positive for both CD80 and CD86. *P < 0.05, **P < 0.01, and ***P < 0.001.

Antitumor Mechanism of CaDM@Surgiflo in vivo

The pH of the normal extracellular environment is approximately 7.2–7.4, while the TME can experience a drop in pH to 6.0–6.5 due to lactic acid accumulation from anaerobic glycolysis. Under acidic conditions, $CaCO_3$ decomposes, releasing DOX to directly kill tumor cells and generating a large amount of Ca^{2+}, inducing calcium overload and subsequent tumor cell death.[37] In vivo calcium content detection showed that Ca^{2+} levels in glioma tissue were significantly increased after CaDM@Surgiflo treatment (Figure S16). Coating with tumor cell membranes provides homologous targeting capability to the nanocarrier, enabling more efficient entry into tumor cells via the EPR effect and endocytosis. As the intracellular pH of tumor cells is further reduced, Ca^{2+} released from intracellular $CaCO_3$ decomposition synergizes with exogenous Ca^{2+} influx, further enhancing the killing effect on tumor cells.[25]

To further investigate the in vivo mechanism, we first performed IHC analysis. As shown in Figure 7A and S17, after CaDM@Surgiflo treatment, HMGB1 expression decreased while CRT expression increased in glioma cells, consistent with in vitro results. Malignant tumors grow rapidly and contain structurally incomplete neovasculature. Ca^{2+}, as a key coagulation factor, can induce thrombosis in tumor blood vessels, blocking nutrient supply and exerting a starvation therapy effect. IHC results showed reduced expression of CD31 and VEGF in the CaDM@Surgiflo group

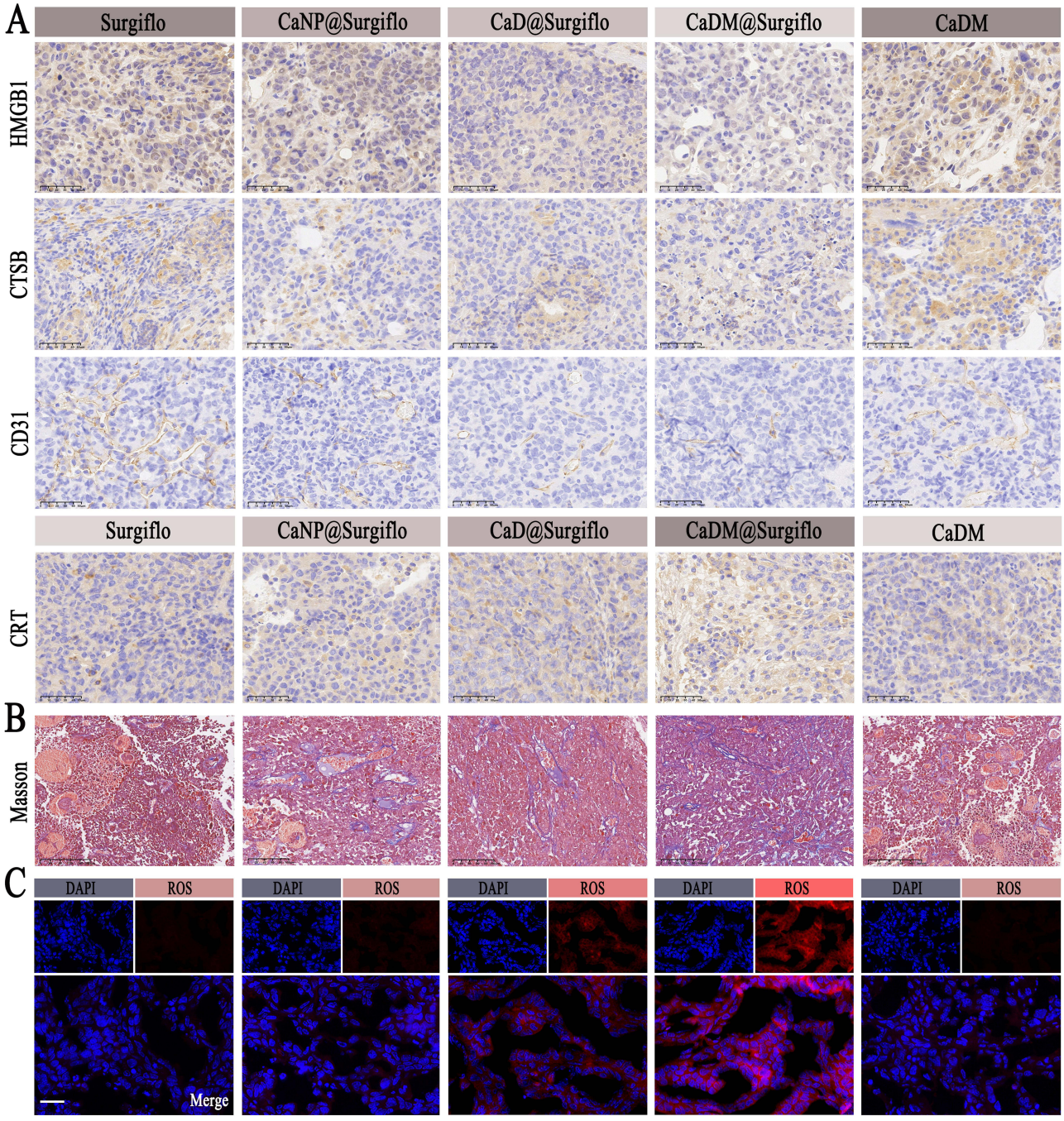

Figure 7 Anti-tumor mechanism of CaDM in vivo. (**A**) Immunohistochemical-stained images of HMGB1, CTSB, CD31 and CRT in tumor tissues from various groups. Scale bar is 50μm. (**B**) Masson-stained images of tumor tissues from various groups. Scale bar is 100μm. (**C**) Fluorescence images of ROS in tumor tissues from various groups. Scale bar is 50μm.

(Figures 7A, S18 and S19). Masson and HE staining further indicated a significantly higher proportion of microvascular thrombosis in the tumor tissues of this treatment group (Figures 7B and S20). Studies have shown that increasing TME pH can reduce the expression of cathepsin B (CTSB), a key molecule promoting tumor invasion, metastasis, and angiogenesis, which is closely associated with poor prognosis in gliomas and other malignancies.[38] In this study, CTSB expression was significantly downregulated in glioma tissues after CaDM@Surgiflo treatment (Figure 7A), thereby inhibiting endothelial cell migration and tumor angiogenesis and enhancing the antitumor effect. Additionally, elevated CTSB activity in the acidic microenvironment can degrade immune-related molecules such as

https://doi.org/10.2147/IJN.S578002

MHC, suppressing T cell and NK cell function and promoting immune escape. The reduction in CTSB expression favors the remodeling of the immunosuppressive TME.

As a type I ICD inducer, DOX can induce mild endoplasmic reticulum stress and release DAMPs.[39] This study also found that Ca^{2+} released from $CaCO_3$ decomposition triggers calcium overload, further leading to ROS accumulation. As shown in Figure 7C, ROS levels in tumor cells of the CaDM@Surgiflo group were significantly elevated, creating conditions for ICD induction. DOX and calcium overload act synergistically to promote ICD.[16,19]

Immune Response Activation and Clinical Translation Potential

To evaluate in vivo immune responses, immunofluorescence staining revealed a markedly increased number of DCs in tumor tissues from the CaDM@Surgiflo group (Figure 8A). Flow cytometry further confirmed a significant elevation of mature DCs in this group (Figure 8B). Meanwhile, the infiltration of $CD8^+$ and $CD4^+$ T cells was substantially increased (Figures 8C and S21), whereas the proportion of Tregs was significantly reduced (Figure 8D). Quantitative analyses of the flow cytometry data further supported these trends, showing an increased proportion of mature DCs (Figure 8E), enhanced infiltration of $CD8^+$ and $CD4^+$ T cells (Figure 8F), and a decreased proportion of Tregs (Figure 8G) in the CaDM@Surgiflo group. In addition, TNF-α and IFN-γ levels in tumor tissues were markedly upregulated (Figure 8H and I). Collectively, these results demonstrate that CaDM@Surgiflo effectively induces ICD in vivo and remodels the tumor immune microenvironment, thereby suppressing postoperative glioma recurrence.

The local delivery of drugs using nanomaterials and hydrogels into the postoperative glioma cavity has been established as an effective strategy to inhibit recurrence.[40] However, the clinical translation of this approach faces challenges related to the biosafety of the carriers and the stability of therapeutic efficacy. The $CaCO_3$ nanomaterial used in this study, composed primarily of calcium, exhibits excellent biocompatibility and degradability, and has shown promising potential in biomedical applications in recent years.[11,41] Although anthracyclines, including DOX, are effective ICD inducers, their systemic toxicity limits clinical application.[16] The release of Ca^{2+} from $CaCO_3$ also acts as a novel ICD inducer.[42] Local delivery of DOX via $CaCO_3$ carriers may enhance efficacy while reducing systemic toxicity. Furthermore, $CaCO_3$ degrades responsively in the acidic tumor microenvironment, releasing both DOX and Ca^{2+} to achieve multi-mechanistic synergistic antitumor effects, including ICD induction. The use of Surgiflo hemostatic gelatin, a clinically approved material, as an alternative to hydrogels for nanoparticle delivery, not only provides hemostasis but also optimizes spatial distribution of the nanoparticles due to its adhesive properties, improving therapeutic outcomes. Simultaneously, the gradual absorption of Surgiflo enables sustained drug release, prolonging the duration of antitumor action. This study validates the efficacy of combining $CaCO_3$ nanoparticles with Surgiflo, providing a new rationale for its clinical translation and offering novel insights for the prevention and control of postoperative glioma recurrence.

This study still has several limitations. First, although the gas-diffusion method is relatively straightforward, its reaction kinetics are slow and highly sensitive to process conditions, which may limit yield and compromise batch-to-batch consistency; future improvements in scalability could be achieved through process engineering and parameter standardization. Second, the as-prepared $CaCO_3$ nanoparticles still have room for optimization in terms of size uniformity and colloidal stability, and further formulation and process optimization may enhance size controllability and long-term stability to meet the requirements of large-scale manufacturing and quality control. In addition, the stability of membrane extraction and coating, the integrity of membrane structure/proteins, and the uniformity of the coating can all influence homologous targeting and in vivo behavior, thereby affecting therapeutic efficacy; therefore, a more rigorous quality-control and stability-evaluation framework is warranted, together with more controllable and reproducible coating and storage protocols to reduce inter-batch variation. Finally, although calcium is an essential element, locally high Ca^{2+} doses may still pose potential risks such as coagulation abnormalities and fluctuations in blood calcium levels; thus, local dosing and release kinetics require finer control, and more systematic evaluation of the dose–efficacy–safety window and toxicology should be performed in future studies. Overall, continued optimization focusing on scalable fabrication, batch consistency, membrane-coating quality control, and safety assessment will facilitate further translational development of this localized therapeutic strategy.

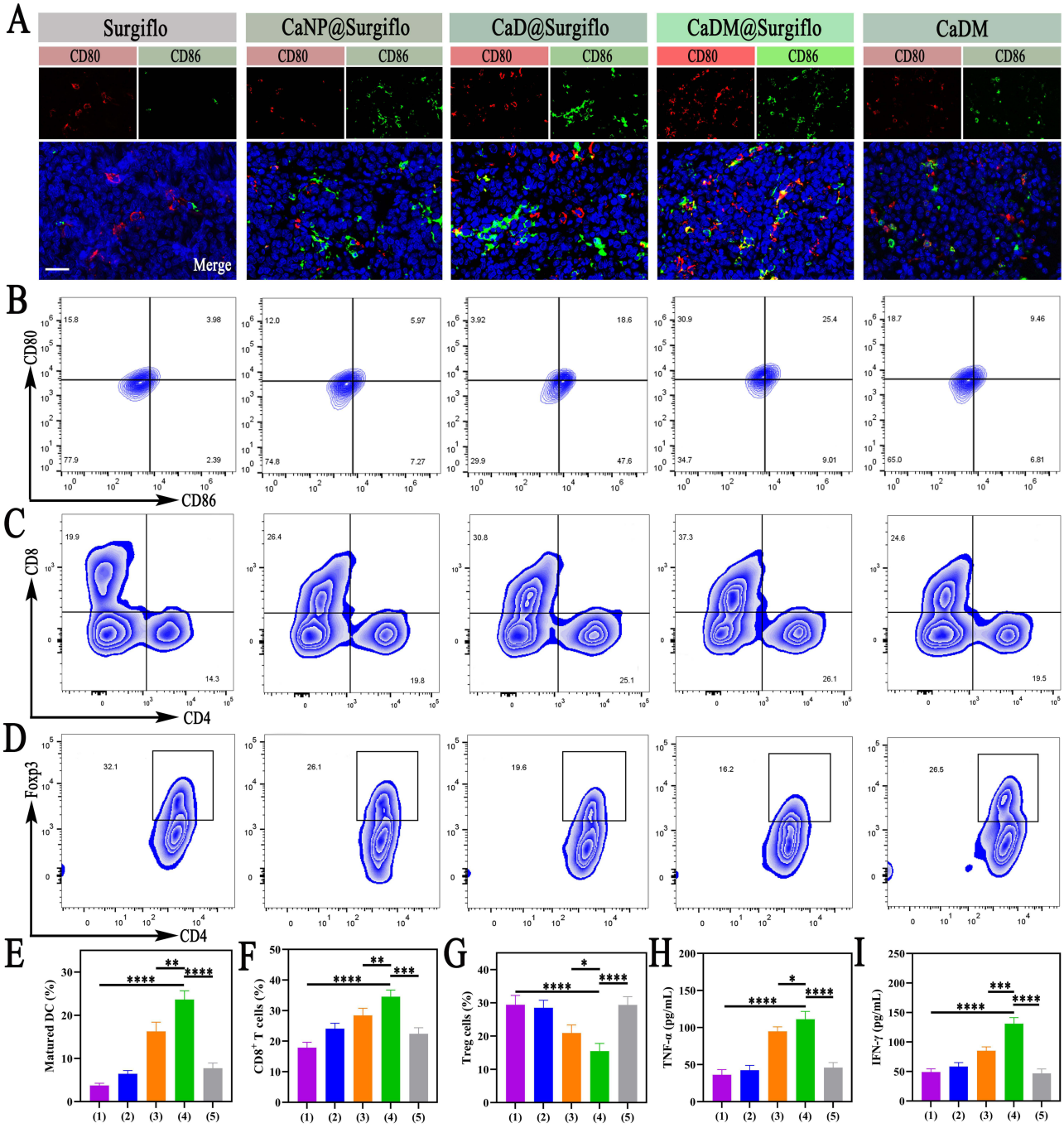

Figure 8 Activation of ICD by CaDM in vivo. (**A**) Fluorescence images of CD80 and CD86 in tumor tissues from various groups. Scale bar is 50μm. (**B**) Flow cytometry analysis of CD80 and CD86 for DC maturation, and (**E**) Semi-quantitative statistical analysis in various groups. (**C**) Flow cytometry analysis of $CD4^+$ and $CD8^+$ T cells, and (**F**) Semi-quantitative statistical analysis in various groups. (**D**) Flow cytometry analysis of Treg cell, and (**G**) Semi-quantitative statistical analysis in various groups. Secretion levels of TNF-α (**H**) and IFN-γ (**I**) in glioma tissues in various groups. (1) Surgiflo, (2) CaNP@Surgiflo, (3) CaD@Surgiflo, (4) CaNP@Surgiflo, (5) CaDM. The black box denotes cells that are double-positive for both Foxp3 and CD4. *P < 0.05, **P < 0.01, ***P < 0.001, and ****P < 0.0001.

Conclusions

In this study, we successfully developed CaDM, a targeted drug delivery system with favorable biosafety and biocompatibility, and demonstrated that its localized application in the postoperative glioma recurrence model—via combination with the clinically used hemostatic material Surgiflo—remarkably suppressed tumor recurrence. Compared with conventional therapeutic regimens as well as non-targeted delivery systems lacking microenvironment-responsiveness, our

https://doi.org/10.2147/IJN.S578002

nanotechnology-based strategy provides improved therapeutic outcomes by enabling localized, on-demand release and multi-mechanistic synergistic immunoactivation. First, Surgiflo facilitates retention within the resection cavity and sustained local release, thereby increasing effective drug exposure at residual tumor sites while reducing systemic exposure. Second, CaDM undergoes acid-responsive degradation in the mildly acidic tumor microenvironment, which not only elevates local pH and downregulates CTSB expression to alleviate the immunosuppressive milieu, but also synchronously releases DOX and Ca^{2+} to achieve cooperative antitumor effects. Mechanistically, DOX directly damages tumor cell DNA and induces immunogenic cell death (ICD). Meanwhile, Ca^{2+} contributes to antitumor efficacy through two complementary routes: (i) acting as a coagulation-related factor that promotes intratumoral thrombosis in neovasculature, thereby restricting nutrient supply and exerting a "starvation-like" effect; and (ii) triggering calcium overload–mediated mitochondrial dysfunction, which further amplifies ICD-associated signals. Consequently, these coordinated effects promote dendritic cell maturation and enhance T cell–mediated antitumor immune responses. Collectively, our integrated strategy—combining a biomimetic cell membrane–coated inorganic $CaCO_3$ nanoplatform with a clinically applicable local carrier—enhances local postoperative control and immune remodeling, offering a translationally promising approach and experimental evidence for preventing glioma recurrence after surgery.

Data Sharing Statement

The data are available from the corresponding author (Ning Lin).

Ethics Approval and Consent to Participate

This study was approved by the Ethics Committee of Anhui Medical University.

Consent for Publication

All authors approved the submission to this journal.

Acknowledgments

This work was supported by Scientific Research Foundation of Education Department of Anhui Province (2024AH040093, 2025AHGXZK50002, 2025AHGXZK50153), Chuzhou Science and Technology Program (2024YF007); Health Research Program of Chuzhou (CZWJ2024A001).

Author Contributions

All authors made a significant contribution to the work reported, whether that is in the conception, study design, execution, acquisition of data, analysis and interpretation, or in all these areas; took part in drafting, revising or critically reviewing the article; gave final approval of the version to be published; have agreed on the journal to which the article has been submitted; and agree to be accountable for all aspects of the work.

Disclosure

The authors report no conflicts of interest in this work.

References

1. Hou S, Jin C, Yang M, et al. Prognostic value of hematologic prealbumin/fibrinogen ratio in patients with glioma. *World Neurosurg*. 2022;160:e442–e453. doi:10.1016/j.wneu.2022.01.048
2. Alhalabi OT, Fletcher MNC, Hielscher T, et al. A novel patient stratification strategy to enhance the therapeutic efficacy of dasatinib in glioblastoma. *Neuro Oncol*. 2022;24(1):39–51. doi:10.1093/neuonc/noab158
3. Xu S, Tang L, Li X, Fan F, Liu Z. Immunotherapy for glioma: current management and future application. *Cancer Lett*. 2020;476:1–12. doi:10.1016/j.canlet.2020.02.002
4. Tonn JC, Thon N, Schnell O, Kreth FW. Personalized surgical therapy. *Ann Oncol*. 2012;23(Suppl 10):x28–32. doi:10.1093/annonc/mds363
5. Grippin AJ, Lee D, Parkes EE, Jiang W, Kim BYS. Nanotechnology for immuno-oncology. *Nat Cancer*. 2025;6(8):1311–1325. doi:10.1038/s43018-025-01025-x
6. Yang C, Ming H, Li B, et al. A pH and glutathione-responsive carbon monoxide-driven nano-herb delivery system for enhanced immunotherapy in colorectal cancer. *J Control Release*. 2024;376:659–677. doi:10.1016/j.jconrel.2024.10.043

7. Ando H, Ikeda A, Tagami M, et al. Oral administration of sodium bicarbonate can enhance the therapeutic outcome of Doxil(R) via neutralizing the acidic tumor microenvironment. *J Control Release*. 2022;350:414–420. doi:10.1016/j.jconrel.2022.08.031
8. Khan O, Chaudary N. The use of amikacin liposome inhalation suspension (Arikayce) in the treatment of refractory nontuberculous mycobacterial lung disease in adults. *Drug Des Devel Ther*. 2020;14:2287–2294. doi:10.2147/DDDT.S146111
9. Ren Y, Yang H, Xu D, Zhang Z, Gao S, Yu R. Application of multifunctional metal nanoparticles in the treatment of glioma. *Int J Nanomed*. 2025;20:625–638. doi:10.2147/IJN.S493565
10. Wang K, Sun J, Zhao H, et al. Advances and challenges in nano-delivery systems for glioblastoma treatment: a comprehensive review. *Int J Nanomed*. 2025;20:9597–9620. doi:10.2147/IJN.S531451
11. Dong Z, Liu Y, Wang C, et al. Tumor microenvironment modulating CaCO(3) -based colloidosomal microreactors can generally reinforce cancer immunotherapy. *Adv Mater*. 2024;36(9):e2308254. doi:10.1002/adma.202308254
12. Wang C, Dong Z, Hao Y, et al. Coordination polymer-coated CaCO(3) reinforces radiotherapy by reprogramming the immunosuppressive metabolic microenvironment. *Adv Mater*. 2022;34(3):e2106520. doi:10.1002/adma.202106520
13. Dong Z, Feng L, Zhu W, et al. CaCO(3) nanoparticles as an ultra-sensitive tumor-pH-responsive nanoplatform enabling real-time drug release monitoring and cancer combination therapy. *Biomaterials*. 2016;110:60–70. doi:10.1016/j.biomaterials.2016.09.025
14. Lin C, Akhtar M, Li Y, Ji M, Huang R. Recent developments in CaCO(3) nano-drug delivery systems: advancing biomedicine in tumor diagnosis and treatment. *Pharmaceutics*. 2024;16(2):275. doi:10.3390/pharmaceutics16020275
15. Zhao P, Tian Y, Lu Y, et al. Biomimetic calcium carbonate nanoparticles delivered IL-12 mRNA for targeted glioblastoma sono-immunotherapy by ultrasound-induced necroptosis. *J Nanobiotechnology*. 2022;20(1):525. doi:10.1186/s12951-022-01731-z
16. Bai S, Lan Y, Fu S, Cheng H, Lu Z, Liu G. Connecting calcium-based nanomaterials and cancer: from diagnosis to therapy. *Nanomicro Lett*. 2022;14(1):145. doi:10.1007/s40820-022-00894-6
17. Xue CC, Li MH, Zhao Y, et al. Tumor microenvironment-activatable Fe-doxorubicin preloaded amorphous CaCO(3) nanoformulation triggers ferroptosis in target tumor cells. *Sci Adv*. 2020;6(18):eaax1346. doi:10.1126/sciadv.aax1346
18. Zhang C, Li S, Yu A, Wang Y. Nano CaCO(3) "Lysosomal Bombs" enhance chemotherapy drug efficacy via rebalancing tumor intracellular pH. *ACS Biomater Sci Eng*. 2019;5(7):3398–3408. doi:10.1021/acsbiomaterials.9b00436
19. Zhu Y, Yang Z, Dong Z, et al. CaCO(3)-assisted preparation of pH-responsive immune-modulating nanoparticles for augmented chemo-immunotherapy. *Nanomicro Lett*. 2020;13(1):29. doi:10.1007/s40820-020-00549-4
20. Lin M, Li Y, Long H, et al. Cell membrane-camouflaged DOX-loaded beta-glucan nanoparticles for highly efficient cancer immunochemotherapy. *Int J Biol Macromol*. 2023;225:873–885. doi:10.1016/j.ijbiomac.2022.11.152
21. Fang RH, Gao W, Zhang L. Targeting drugs to tumours using cell membrane-coated nanoparticles. *Nat Rev Clin Oncol*. 2023;20(1):33–48. doi:10.1038/s41571-022-00699-x
22. Zeng Y, Li S, Zhang S, Wang L, Yuan H, Hu F. Cell membrane coated-nanoparticles for cancer immunotherapy. *Acta Pharm Sin B*. 2022;12(8):3233–3254. doi:10.1016/j.apsb.2022.02.023
23. Jiang Y, Krishnan N, Zhou J, et al. Engineered cell-membrane-coated nanoparticles directly present tumor antigens to promote anticancer immunity. *Adv Mater*. 2020;32(30):e2001808. doi:10.1002/adma.202001808
24. Gravan P, Marchal JA, Galisteo-Gonzalez F. Improving tumor treatment: cell membrane-coated nanoparticles for targeted therapies. *Mater Today Bio*. 2025;32:101716. doi:10.1016/j.mtbio.2025.101716
25. Li Y, Zhou S, Song H, Yu T, Zheng X, Chu Q. CaCO(3) nanoparticles incorporated with KAE to enable amplified calcium overload cancer therapy. *Biomaterials*. 2021;277:121080. doi:10.1016/j.biomaterials.2021.121080
26. Nance E, Zhang C, Shih TY, Xu Q, Schuster BS, Hanes J. Brain-penetrating nanoparticles improve paclitaxel efficacy in malignant glioma following local administration. *ACS Nano*. 2014;8(10):10655–10664. doi:10.1021/nn504210g
27. Chen S, Qiu Q, Wang D, et al. Dual-sensitive drug-loaded hydrogel system for local inhibition of post-surgical glioma recurrence. *J Control Release*. 2022;349:565–579. doi:10.1016/j.jconrel.2022.07.011
28. Lillehei KO, Kalkanis SN, Liau LM, et al. Rationale and design of the 500-patient, 3-year, and prospective vigilant observation of GlIadeL WAfer ImplaNT registry. *CNS Oncol*. 2018;7(2):CNS08. doi:10.2217/cns-2017-0036
29. Roux A, Peeters S, Zanello M, et al. Extent of resection and Carmustine wafer implantation safely improve survival in patients with a newly diagnosed glioblastoma: a single center experience of the current practice. *J Neurooncol*. 2017;135(1):83–92. doi:10.1007/s11060-017-2551-4
30. Ding L, Wang Q, Shen M, et al. Thermoresponsive nanocomposite gel for local drug delivery to suppress the growth of glioma by inducing autophagy. *Autophagy*. 2017;13(7):1176–1190. doi:10.1080/15548627.2017.1320634
31. Wang X, Ye L, He W, et al. In situ targeting nanoparticles-hydrogel hybrid system for combined chemo-immunotherapy of glioma. *J Control Release*. 2022;345:786–797. doi:10.1016/j.jconrel.2022.03.050
32. Cao X, Li S, Chen W, et al. Multifunctional hybrid hydrogel system enhanced the therapeutic efficacy of treatments for postoperative glioma. *ACS Appl Mater Interfaces*. 2022;14(24):27623–27633. doi:10.1021/acsami.2c05147
33. Meng J, Chen M, Gu F, et al. In situ formed chemo-immunotherapeutic hydrogel for suppression of postoperative glioma recurrence and intraoperative hemostasis. *J Control Release*. 2025;387:114168. doi:10.1016/j.jconrel.2025.114168
34. Hsu CY, Lin J, Wei MF, Chen LH, Liang HT, Lin FH. Local delivery of carboplatin-loaded hydrogel and calcium carbonate enables two-stage drug release for limited-dose radiation to eliminate mouse malignant glioma. *Biomaterials*. 2025;312:122746. doi:10.1016/j.biomaterials.2024.122746
35. Danker W 3rd, Aggarwal J, Kelkar SS, Marston XL, Gao X, Johnston SS. Real-world clinical and economic outcomes associated with Surgiflo((R)) vs floseal in cardiovascular surgeries in the US. *Clinicoecon Outcomes Res*. 2022;14:129–138. doi:10.2147/CEOR.S338672
36. Nie D, Ling Y, Lv W, et al. In situ attached photothermal immunomodulation-enhanced nanozyme for the inhibition of postoperative malignant glioma recurrence. *ACS Nano*. 2023;17(14):13885–13902. doi:10.1021/acsnano.3c03696
37. Zhao Y, Luo Z, Li M, et al. A preloaded amorphous calcium carbonate/doxorubicin@silica nanoreactor for pH-responsive delivery of an anticancer drug. *Angew Chem Int Ed Engl*. 2015;54(3):919–922. doi:10.1002/anie.201408510
38. Natan Y, Blum YD, Arav A, et al. Amorphous calcium carbonate shows anti-cancer properties that are attributed to its buffering capacity. *Cancers*. 2023;15(15).
39. Huang FY, Lei J, Sun Y, et al. Induction of enhanced immunogenic cell death through ultrasound-controlled release of doxorubicin by liposome-microbubble complexes. *Oncoimmunology*. 2018;7(7):e1446720. doi:10.1080/2162402X.2018.1446720

40. Zhang J, Chen C, Li A, et al. Immunostimulant hydrogel for the inhibition of malignant glioma relapse post-resection. *Nat Nanotechnol*. 2021;16 (5):538–548. doi:10.1038/s41565-020-00843-7
41. Huang J, He J, Wang J, et al. Calcium carbonate-actuated ion homeostasis perturbator for oxidative damage-augmented Ca(2+)/Mg(2+) interference therapy. *Biomaterials*. 2023;302:122340. doi:10.1016/j.biomaterials.2023.122340
42. Zheng P, Ding B, Jiang Z, et al. Ultrasound-augmented mitochondrial calcium ion overload by calcium nanomodulator to induce immunogenic cell death. *Nano Lett*. 2021;21(5):2088–2093. doi:10.1021/acs.nanolett.0c04778